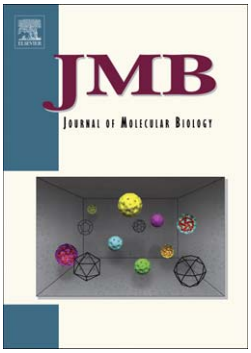

Transition path times measured by single-molecule spectroscopy

Hoi Sung Chung

PII: S0022-2836(17)30247-4
DOI: doi:10.1016/j.jmb.2017.05.018
Reference: YJMBI 65420

To appear in: *Journal of Molecular Biology*

Received date: 16 April 2017
Accepted date: 18 May 2017

Please cite this article as: Chung, H.S., Transition path times measured by single-molecule spectroscopy, *Journal of Molecular Biology* (2017), doi:10.1016/j.jmb.2017.05.018

Transition path times measured by single-molecule spectroscopy

Hoi Sung Chung

Laboratory of Chemical Physics, National Institute of Diabetes and Digestive and Kidney Diseases, National Institutes of Health, 5 Memorial Dr., Bethesda, MD 20892-0520.

Correspondence to Hoi Sung Chung: chunghoi@niddk.nih.gov, +1 301-496-0202, (fax) +1 301-496-0850

Abstract

The transition path is a tiny fraction of a molecular trajectory during which the free-energy barrier is crossed. It is a single-molecule property and contains all mechanistic information of folding processes of biomolecules such as proteins and nucleic acids. However, the transition path has been difficult to probe because it is short and rarely visited when transitions actually occur. Recent technical advances in single-molecule spectroscopy have made it possible to directly probe transition paths, which has opened up new theoretical and experimental approaches to investigating folding mechanisms. This article reviews recent single-molecule fluorescence and force spectroscopic measurements of transition path times and their connection to both theory and simulations.

Highlights

- Fluorescence experiment determined average transition path times of protein folding
- Transition path time is insensitive to the free energy barrier height
- Transition path time measurement characterized diffusive barrier crossing dynamics
- Transition path analysis validated 1D description of folding of biomolecules
- Single-molecule force spectroscopy measured distributions of transition path times

Keywords: protein folding, nucleic acid folding, energy landscape, FRET, force spectroscopy

Introduction

The best way to understand mechanisms of chemical and biological reactions is to probe transition states and transition paths. For simple chemical reactions such as chemical bond breaking and formation, the reaction coordinate is usually well-defined and the picture of reaction pathways is relatively clear. On the other hand, in folding reactions of biological macromolecules, such as proteins and nucleic acids consisting of hundreds or thousands of atoms, an immense number of degrees of freedom makes defining transition states and transition paths challenging. However, the problem has been highly simplified by energy landscape theory of protein folding and the postulate that proteins have evolved to reduce the roughness of the energy landscape. Consequently, the reaction coordinate for folding processes can be described with just a few or even a single order parameter (Fig. 1a) [1–7]. In this case, folding of complex biomolecules reduces to the much simpler problem of diffusion of a Brownian particle in a one-dimensional (1D) potential energy surface.

Folding of many single domain two-state proteins, in which only folded and unfolded states are observed in both equilibrium and kinetics experiments, have been successfully explained in this simple picture of diffusion on a one-dimensional free energy profile (Fig. 1b). There are two free energy wells corresponding to the unfolded and folded states separated by a barrier. Then, the folding rate is given by Kramers' theory [10],

$$t_{\mathrm{f}} = \frac{1}{k_{\mathrm{f}}} = \frac{2\pi}{\beta D^{*} \omega^{*} \omega_{\mathrm{u}}} \exp(\beta \Delta G_{\mathrm{f}}^{*}) , \qquad (1)$$

where the folding time t_{f} is the inverse of the rate coefficient k_{f}, D^{*} is the diffusion coefficient at the barrier top, $(\omega^{*})^2$ and $(\omega_{\mathrm{u}})^2$ are the curvatures of the free energy surface at the top of the

barrier and bottom of the unfolded well, respectively, ΔG_f^* is the barrier height, $\beta = 1/k_B T$, k_B is the Boltzmann constant, and T is the absolute temperature. The most widely used experimental method to probe the transition state has been the ϕ-value analysis [11–14]. In this method, the relative changes in the folding equilibrium constant and folding rate coefficient caused by a mutation are interpreted in terms of the extent to which the mutated residue forms the native interactions in the transition state [14].

Instead of indirectly probing the transition state, single molecule spectroscopy potentially allows for a direct access to monitoring structure all along the transition path, not just at the top of the free energy barrier. Fig. 1b shows a molecular trajectory of folding that is observed in single molecule spectroscopy. A molecule spends the vast majority of time in the unfolded state before making a transition over the barrier. This molecular trajectory of barrier crossing corresponds to the transition path. Since molecules undergo merely random fluctuations during long waiting times in the unfolded state, transition paths contain the most important mechanistic information of the process [15,16]. However, transitions occur stochastically (i.e., not synchronized) and cannot be probed by ensemble measurements. On the other hand, by watching one molecule at a time, one can follow a trajectory, isolate transition paths and perform detailed analyses. The difficulty in the experiment has been the relatively poor time resolution of single molecule spectroscopy for measuring this fast event (expected on the μs timescale from all-atom molecular dynamics simulations [17,18]). For the last several years, however, there have been technical advances both in single molecule fluorescence and force spectroscopy, as well as methods of data analysis, to improve the time resolution. In this review, I will describe the first measurement of transition path times and its application to characterizations of the folding energy landscape of proteins and nucleic acids. The current limitations and future directions will also be discussed.

Calculation of transition path times

The transition path on a 1D free energy surface is defined rigorously as the part of a molecular trajectory that leaves a position of coordinate q_u of the unfolded side of the barrier and reaches q_f on the other side without re-crossing q_u (brown portion of the trajectory in Fig. 1b). The exact value of the average transition path time, t_{TP} can be computed for a barrier with an arbitrary shape from [19]

$$t_{TP} = \frac{1}{D^*}\int_{q_u}^{q_f} e^{-\beta G(q)}\phi_f(q)(1-\phi_f(q))dq\int_{q_u}^{q_f} e^{\beta G(q')}dq' . \qquad (2)$$

Here, $\phi_f(q) = \int_{q_u}^{q} e^{\beta G(q')}dq' \Big/ \int_{q_u}^{q_f} e^{\beta G(q')}dq'$ is the splitting probability for folding that is defined as the fraction of trajectories that start from q and reach q_f before reaching q_u. Because of microscopic reversibility, the transition path time from q_u to q_f is the same as that from q_f to q_u. For a high ($\beta\Delta G^*$ >> 1) parabolic barrier, Eq. (2) becomes [16,20]

$$t_{TP} = \frac{1}{\beta D^*(\omega^*)^2}\ln(2e^{\gamma}\beta\Delta G^*) , \qquad (3)$$

where γ (= 0.577 …) is Euler's constant.

In addition to the average transition path time, the distribution of the transition path times can be found for a high parabolic barrier [21],

$$P(t) = \frac{\beta D^*(\omega^*)^2\sqrt{\beta\Delta G^*}}{1-\mathrm{erf}(\sqrt{\beta\Delta G^*})} \frac{\exp\left[-\beta\Delta G^* \coth(\beta D^*(\omega^*)^2 t/2)\right]}{\sinh(\beta D^*(\omega^*)^2 t/2)\sqrt{2\pi\sinh(\beta D^*(\omega^*)^2 t)}}, \quad (4)$$

where erf(x) is the error function. Since Eq. (4) is obtained with the open boundary condition at q_u (in other words, re-crossing at the starting position q_u is allowed), the average transition path time calculated using Eq. (4) is longer than the value by Eqs. (2) and (3). As the barrier height increases, the effect of re-crossing at q_u becomes smaller and the value converges to the exact value. The average transition path times calculated using Eqs. (2) – (4) are compared in Fig. 2c.

Single molecule fluorescence experiments

Transition path time is insensitive to the barrier height

In single molecule Förster resonance energy transfer (FRET) spectroscopy, molecules are immobilized on a surface to measure photon trajectories for monitoring folding and unfolding transitions (Fig. 1c). For protein folding, for example, the experiment is carried out near the mid-point of denaturation, where a molecule spends equal amount of time in the two states. The folded and unfolded states are distinguished by the apparent FRET efficiency, the fraction of detected photons that are emitted by the acceptor. Although it depends on the labeling positions of donor and acceptor fluorophores, the FRET efficiency is usually higher (more acceptor photons) in the folded state than in the unfolded state.

As mentioned in Introduction, the difficulty in the measurement of transition path times is the relatively poor time resolution of single molecule FRET spectroscopy. This problem has been overcome by collecting photon trajectories at high illumination intensity and employing a statistical analysis [22]. Figure 3(a) shows donor and acceptor trajectories with a photon count rate of ~ 800 photons/ms. Even at this high photon count rate (the average photon interval is 1.2

μs), the transition still looks instantaneous. In other words, the transition path time is shorter than the bin time, 50 μs, and individual transition path times cannot be measured. To improve the time resolution, the authors directly analyzed photon trajectories without binning using the Gopich-Szabo maximum likelihood method [23]. If the transition path time is sufficiently long that a certain number of photons are detected during transitions, the average transition path time can be determined by a collective analysis of a large number of photon trajectories. In this analysis, a three-state model was used (Fig. 3b), which consists of the folded and unfolded states and a virtual intermediate state at the top of the free energy barrier. The lifetime of this virtual state (τ_S) (the reciprocal of the sum of the rate coefficients for the transition from the top of the barrier to the folded and unfolded states) corresponds to the average transition path time, t_{TP}. By comparing the likelihood value $L(\tau_S)$ with that of the two-state model with an instantaneous transition ($L(0)$), it is possible to state whether the transition path time is determined with a certain statistical significance or only the upper bound can be determined. In this analysis, confirmed by simulations of photon trajectories, the time corresponding to the maximum of the difference of the log-likelihood $\Delta \ln L = \ln L(\tau_S) - \ln L(0)$ is the average transition path time, t_{TP}.

Equation 3 predicts that the transition path time depends logarithmically on the free energy barrier height (ΔG^*) and, in sharp contrast to the folding time (Eq. (1)), is insensitive to ΔG^*. This prediction was tested by comparing folding and transition path times for a fast (FBP28 WW domain) and a slow (protein GB1) folding protein (fast and slow folding in terms of kinetics). For FBP28 (Fig. 3c), a peak was found at τ_S = 16 μs in the likelihood plot, which was measured in 50% glycerol solution (viscosity of 10 cP) to slow both the folding and transition path times. Since the folding time was slowed 10-fold and all of the viscosity dependence for both folding and transition path times is contained in the diffusion coefficient D^* (Eqs. (1) and

(3)), the transition path time is also slowed 10-fold and is therefore 10 times shorter, ~ 2 μs, in water [22]. This time is consistent with the earlier results and predictions. Gruebele and coworkers measured the timescale of the 'molecular phase' of the λ-repressor and the FiP35 WW domain [24,25]. Prior to the major folding/unfolding relaxation of 10 – 20 μs, they observed ~ 2 μs decay, which was attributed to the relaxation from the barrier top. For these proteins, the barrier top is significantly populated due to the low barrier height so that it can be measured in ensemble experiments. This timescale corresponds to the pre-exponential factor in Eq. (1), which would be the folding time when there is no barrier and can be considered as the "speed limit" of protein folding [24,26,27]. If the curvatures and the diffusion coefficient at the barrier top and the bottom of unfolded well are similar, the pre-exponential factor of Eq. (1) becomes $2\pi\tau_r$, where τ_r is the reconfiguration time of unfolded proteins [27,28]. With the reconfiguration time of 50 – 100 ns [29,30], the pre-exponential factor becomes 0.3 – 0.6 μs, which is close to the timescales mentioned above. In addition, the single-molecule measurement was similar to the value obtained from a long equilibrium trajectory of an all-atom molecular dynamics (MD) simulation that exhibits multiple transitions so that both the folding rate and transition path time can be determined reliably after a viscosity correction [17].

For the slow-folding protein, protein GB1 was selected, because it had been previously studied in detail to establish criteria for photon trajectories of folding and unfolding free of possible artefacts due to immobilization [16]. The folding kinetics were too slow to collect a sufficient number of transitions at high viscosity. Therefore, only the upper bound of 10 μs was measured (Fig. 3d). Nevertheless, this time is remarkably short and comparable to 2 μs of the WW domain although the folding time (t_f) of the two proteins is vastly different. The ratio of the folding times is 20,000 (= 2 s/100 μs) near the mid-points of denaturation. Using Eqs. (1) and (3)

with the pre-exponential factor of 1 μs in Eq. (1), the ratio of the transition path times of the two proteins is only 1.4, which is comparable to the experimental measurement of < 5.

The reason for this insensitivity to the barrier height is that the transition path time is a conditional first passage time from q_u to q_f in Fig. 1b. When the barrier is high, most of folding attempts from the unfolded well fail and barrier crossing is a rare event. In other words, for high barriers a trajectory that leaves q_u goes back to q_u in almost every case (Fig. 1b). The time for this process is added to the waiting time in the unfolded state, the inverse of which is the folding rate coefficient. When this happens, the clock for the transition path time is reset. A transition path requires a series of successive, lucky thermal kicks to propel the system over the barrier, which is not so different whether the barrier is high or low.

Characterization of diffusion at the barrier top

In solution, protein molecules are solvated by water molecules, and it is reasonable to assume that the diffusion coefficient of a molecular process is inversely proportional to the solvent viscosity according to the Stokes-Einstein relation. In this case, the folding diffusion coefficient (D^*) of Eqs. (1) and (3) may not differ much between proteins, predicting that the transition path time would be very similar for all proteins. However, there are exceptions. For example, in addition to solvent friction, it is possible that solvent-independent friction is present due to the intramolecular interactions of a protein molecule itself, which is called ‘internal friction.’ [31–34] Since the effect of internal friction may be larger at a later stage of the folding process, where proteins become more compact, the diffusion coefficient at the barrier top (D^*) may be different for certain proteins. In the presence of internal friction, D^* is not linearly proportional to the inverse of the solvent viscosity. The nonlinear viscosity dependence has been described by

$$D^* \propto (\sigma + \eta/\eta_0)^{-1}, \quad (5)$$

where (η/η_0) is the relative solvent viscosity and σ is a viscosity term resulting from internal friction, or by an empirical power-law formula

$$D^* \propto (\eta/\eta_0)^{-\alpha}. \quad (6)$$

In order to characterize D^*, one can measure and compare folding kinetics at various solvent viscosities by adding a viscogen and counterbalancing its effect on the free energy difference between the folded and unfolded states, and presumably also the barrier height, by increasing or decreasing the denaturation concentration at each viscogen concentration. The interpretation of the solvent viscosity dependence in this experiment is based on the important assumption that the barrier height does not change by balancing stability at different viscosities so that only the pre-exponential factor (i.e., D^*) in Eq. (1) can be compared. However, the folding time is so sensitive to the barrier height and the effect of its small change on the kinetics can be large. Therefore, the measurement of the transition path time, which is more sensitive to D^* than to the barrier height (Eq. (3)), is a more reliable way to characterize diffusion at the barrier.

For all α-helical proteins, the folding time is less than proportional to the first power of the viscosity ($\alpha < 1$) [31,35–40] because of the presence of internal friction. An unusually large contribution from internal friction was found for the designed protein α_3D (Fig. 1c). Since the presence of internal friction will slow down diffusion, a longer transition path time was expected compared to the two proteins mentioned above. Indeed, the transition path time of α_3D was found to be much longer, 12 μs [9], and it was possible to measure it even without slowing by the addition of a viscogen. This finding made it possible to make the direct and quantitative

comparisons of D^* in various conditions without the interference from the effect of the barrier height. Fig. 4a shows the viscosity and temperature dependence of the transition path time of α_3D. As expected, the transition path time was very insensitive to the solvent viscosity change, suggesting the presence of large internal friction. (Blue dashed line is the case expected when t_{TP} is proportional to the solvent viscosity.)

An interesting phenomenon was observed in the temperature dependence. When the temperature was lowered, the solvent viscosity slightly increased but the transition path time increased much more. This apparently contradicts the very low solvent viscosity dependence in the viscogen experiment above. However, this temperature dependence is a different aspect of landscape roughness (or internal friction) and can be explained theoretically. Although 1D free energy surface is smooth because it is a projection of multi-dimensional energy surface (Fig. 1a), microscopically, a molecule crosses local barriers during diffusion from one position to the next position in the 1D coordinate. Because molecular trajectories are heterogeneous, each molecule experiences different local states and barriers. The average of this effect is reflected in the diffusion coefficient. Bryngelson and Wolynes have shown that the temperature dependence of the diffusion coefficient will follow the super-Arrhenius relation, $D^* \propto \exp[-(\Delta E/k_BT)^2]$, where ΔE^2 is the local mean-squared fluctuation in energy (landscape roughness) [1]. When the roughness is large, the diffusion coefficient as well as the transition path time is very sensitive to the temperature as observed in the experiment. The fit of the data in Fig. 4a results in ΔE = 2.3 k_BT at room temperature.

Structural origin of rough energy landscape and internal friction

One possible reason that the landscape roughness is large for α_3D is that this protein is a designed protein that did not undergo evolution to smooth its folding energy landscape [41].

This protein contains a large number of charged residues: 12 negatively- and 11 positively-charged residues, presenting the possibility that non-native salt bridges may be formed frequently during folding. Breaking these salt bridges during the transition path would cause landscape roughness that would be reflected in D^*. Indeed, the formation of non-native salt bridges during the transition path has been observed in the analysis of the MD simulation by the Shaw group [18,42]. The effect of the salt-bridge formation was investigated in more detail by a combination of single molecule FRET and MD simulations [8].

Experimentally, salt bridges can be easily eliminated by simply lowering the pH below the pKa values of the carboxylic acid groups of glutamate and aspartate. Fig. 4b shows the relaxation rate (sum of the folding and unfolding rates) near the mid-point of urea denaturation at different pHs. The data looks like an acid/base titration curve. The folding rate increases by 14-fold between pH 5.3 and pH 3.2, while the equilibrium constant remains unchanged. This result indicates that the diffusion is much faster at low pH, where non-native salt bridges disappear, as expected. However, this interpretation is based on the assumption that the barrier height does not change over this pH range (same assumption in the experiment of viscosity dependence of folding rates to measure internal friction) and the change in folding rate solely results from the change in D^* in the pre-exponential factor in Eq. (1). The more reliable comparison, therefore, should be made by measuring the transition path times. t_{TP} at pH 5.3 is 13 μs very close to the value at pH 7.6 [9]. However, only an upper bound of 4 μs could be determined at pH 3.6 because the transition path time is too short. Even at 15-times higher viscosity at this pH, an upper bound of 12 μs was measured. With these experimental measurements and simulations of photon trajectories using parameters identical to those of the experiments (count rate distribution, FRET efficiencies of folded and unfolded states, number of transitions), t_{TP} was estimated to be ~ 1 μs at pH 3.6 in aqueous solution. This result indicates that the increase in the folding rate at low pH in Fig. 4b results almost entirely from the increase

of D^* due to the reduced internal friction (or decreased landscape roughness). This interpretation is further supported by the viscosity dependence of the relaxation rates in Fig. 4c, where the inverse of the relaxation rate at pH 3.6 is closer to the inverse first power viscosity dependence than that at pH 7.6. (The less than first power (α<1) at pH 3.6 is discussed below.)

All these experimental observations were also observed in equilibrium folding/unfolding trajectories of all-atom MD simulations by the Shaw group [8]. This includes the faster folding kinetics, shorter transition path times, and higher viscosity dependence at lower pH. This agreement makes the comparison between experimental and simulation results more reliable and makes it possible to look into structural details for the origin of the rough energy landscape of α_3D. Fig. 4d shows the 1D free energy surface constructed from the simulation and the average number of native and non-native salt bridges along the folding coordinate. It shows that a large number of non-native salt bridges are formed during barrier crossing, which is replaced by the native ones as folding proceeds (see also the snapshots of structures). More importantly, Fig. 4e shows that the non-native salt bridges almost disappear at pH 2. After performing various simulations and more detailed analyses to look into other possibilities such as non-native hydrophobic interactions and charge repulsion effect at low pH, the major conclusion from the analysis of the simulations was that non-native salt bridge formation during the transition path is the origin of the slow diffusion during the folding transition over the barrier, consistent with the experimental interpretation.

One unresolved issue in both the simulations and experiments is the origin of α<1 in the viscosity dependence at low pH (Fig. 4c), suggesting there is still additional source of internal friction. Interestingly, the power (α) of 0.70 from the empirical power-law fitting is similar to the values found in the experimental [35] and MD simulation [43] studies of folding of a single α-helix, in which all residues are solvent-exposed, and therefore solvent-excluded friction would be negligible. The low viscosity dependence of α-helix folding has been explained by the

breakdown of Kramers' theory [44], similar to the photoisomerization reaction of small molecules [45]. In α-helix folding, free energy barrier crossing involves dihedral angle rotations of peptide backbone, which is so fast that slow components of the solvent relaxation cannot contribute to energy dissipation. Therefore, the effective friction would be lower than the macroscopic solvent friction, which results in the low viscosity dependence [35,43,46]. On the other hand, the folding time of a β-hairpin scales with the first power of the solvent viscosity because most of backbone dihedral angle rotations to form the β strands occur prior to global free energy barrier crossing [47]. These studies suggest that the reduced viscosity dependence of α_3D folding at low pH is an intrinsic property of α-helix folding.

Similar to folding of a single α-helix, it was puzzling to observe the highly non-linear viscosity dependence at neutral pH because most of the charged residues involved in the non-native salt-bridge formation are solvent-exposed in the simulation. In this case, the energy landscape can be rough but this does not necessarily cause reduced solvent-viscosity dependence. Further simulations by the Shaw group for the formation of ion pairs that are fully solvated and resemble the salt-bridge formation provided a clue on this issue [8]. They found that the persistence time of various ion pairs including charged side chains of amino acid residues showed reduced viscosity dependence similar to α-helix folding. The weak viscosity dependence arises from the last reorganization step of the pair formation. To summarize the molecular interpretations for the experimental observations of α_3D [9], the very weak solvent-viscosity dependence of α_3D folding at neutral pH results from the two non-Markovian effects of α-helix folding and salt-bridge formation, whereas the sensitive temperature dependence of the transition path time [9] results from the landscape roughness caused by non-native salt bridges.

Single molecule force experiments

Measurement of transition path times by landscape reconstruction

There are various ensemble and single-molecule methods that can measure the folding kinetics accurately. However, it is very difficult to determine the barrier height from the folding rate because the parameters in the pre-exponential factor in Eq. (1) including the diffusion coefficient and the curvatures are not known. By measuring the folding rate and transition path time together in the fluorescence measurement above, the barrier height has been determined with a reasonable accuracy using the curvature values obtained from MD simulation [9]. On the other hand, in single molecule force spectroscopy (Fig. 5a), the pulling coordinate is the reaction coordinate and it is possible to reconstruct a 1D free-energy surface along the molecular extension from the experimental measurements of the total extension [48–53]. Using deconvolution techniques, the barrier height (ΔG_f^*) and curvatures at the top of the barrier and bottom of the wells, $(\omega^*)^2$ and $(\omega_u)^2$, can be determined. In addition to these parameters, if D^* is obtained from the measured rate coefficient (k_f) between the two states using Eq. (1), one can calculate the average transition path time from Eq. (3) using the same parameters.

Woodside and coworkers have used this approach to determine the average transition path times of various systems, including DNA hairpins, RNA pseudoknots, a riboswitch [54], and the prion protein [55]. Similar to single molecule fluorescence measurements for protein folding [22], they showed that the transition path times of different nucleic acids are all on the order of tens of microseconds regardless of their topologies and the number of base pairs in the stem of hairpins, while their folding rates differ by many orders of magnitude. This result shows that the 1D diffusion theory, from which Eq. (1) and (3) were derived, describes folding of these biomolecules very well. The 1D theory has been further validated by single-molecule fluorescence measurement of the transition path time (upper bound) of a shorter DNA hairpin [56]. Woodside and coworkers also described a procedure to reconstruct the barrier region of

the free energy surface using the folding probability at a particular position in the coordinate, $p_{fold}(q)$ (i.e., splitting probability $\phi_f(q)$ in Eq. (2)) [19,57], which would not need a deconvolution procedure [58].

It should be noted that there has been a remarkable improvement of the time resolution in another single molecule force technique, atomic force microscopy. By using ultrashort cantilevers [59], Yu *et al*. have observed a large number of intermediate states with a lifetime of 10 μs or sometimes shorter during complex mechanical unfolding of a membrane protein, bacteriorhodopsin [60]. Similar to the optical tweezers experiments above, they could reconstruct a free energy barrier between two intermediate states by deconvolution and using the measured splitting probabilities.

Direct measurement of individual transition paths

Recently, Woodside and coworkers have improved the time resolution of the single-molecule force technique and measured transition path times of individual transitions of folding of DNA hairpins and misfolding of the prion protein for the first time (Fig. 5b) [61–63]. This remarkable achievement has opened up the possibilities of various new investigations in theory, simulation, and experiments.

Analysis of the distribution of the transition path time is one example. The distribution of the transition path times of folding and unfolding of a DNA hairpin is shown in Fig. 5c. The average transition path time is 28 μs, which is consistent with the previous indirect measurement using the landscape reconstruction method as described above [54]. However, the width of the distribution is much wider than the width expected from the free energy barrier height of 9.1 k_BT from the landscape reconstruction. In particular, the fraction of short transition path times is too large (compare Fig. 2b and 5c). Fitting the distribution to Eq. (4) results in the barrier height of only 0.4 k_BT, which seems very unlikely because of the slow kinetics. (The

mean transition path time by Eq. (4) is actually ~ 2.5 times longer than the exact value for this low barrier height (Fig. 2c).)

This discrepancy can result from various factors such as deviation from the 1D theory, anharmonicity of the barrier [63], and the unwanted influence from the bead and DNA handles [64–67]. There have already been theoretical considerations of this issue. Pollak pointed out that Eq. (4) was derived with the free (open) boundary condition as mentioned above, while the experimental distribution was obtained using absorbing boundary condition (Fig. 5b) [68]. Since the open boundary condition allows the re-crossing at the boundary, the tail part of the distribution becomes broader, which results in the lower apparent barrier height. The barrier height from the boundary to the top of the barrier is also lower than the height from the bottom of the well to the top of the barrier (Fig. 1b). However, this would explain only a fraction of the difference between 0.4 k_BT and 9.1 k_BT. Makarov also discussed that the 1D Smoluchowski model does not work for describing the average transition path time and its distribution when the free energy barrier is largely due to entropy, while it still predicts an accurate rate coefficient [69]. However, the discrepancy was not explained completely, and it is still an open question.

In the recent work, Neupane *el al*. have studied the sequence dependence of the diffusion coefficient of DNA hairpin folding by measuring the distribution of the transition path times [63]. The diffusion coefficient is linearly proportional to the content of the G:C base pair, suggesting that the roughness of folding energy landscape depends on the sequence, similar to that of protein folding [8].

Limitations and future directions

The ultimate goal of studying transition paths would be to obtain three-dimensional structural information during the transition path to compare with the results of all-atom MD simulations and

the prediction of analytical models. For this purpose, major technological improvements will be required for both fluorescence and force techniques.

First, the time resolution of the measurement should be further improved. In single molecule fluorescence spectroscopy, the time resolution is determined by the photon detection rate, which is proportional to laser illumination intensity. At high laser intensity, the complex photophysics of fluorophores such as photoblinking and photobleaching make the measurement difficult and complicate the interpretation. The rate of photobleaching increases roughly as the square of the photon count rate, which markedly shortens the trajectory at high illumination intensity. Photoblinking, during which no information can be obtained, also increases proportional to the illumination intensity. With various chemical cocktails to suppress these processes, the average length of the trajectory is 0.5 – 1 ms and the dark state population is 5 – 10% at the photon count rate of 500 – 1000 photons/ms that is required for measuring the average transition path time longer than 10 μs. In the measurement of the average transition path time, it is possible to incorporate acceptor blinking into the kinetic model [8,20,70,71], but this would be more complicated in the analysis of individual transition paths. Another way to enhance the time resolution is to slow down the folding process instead of increasing the photon count rate. So far, the viscosity has been increased up to 50 times higher than water viscosity for this measurement [9]. However, dye photophysics problems also become worse as the viscosity is increased. This experiment may need some magic cocktail or different kind of dyes with appropriate chemical modifications similar to 'self-healing' dyes to reduce photoblinking and photobleaching effects [72–74].

Recently, instead of simply raising illumination intensity, an alternative approach has been studied to increase photon count rate using the plasmonic enhancement of fluorescence. It has been shown that fluorescence emission can be enhanced by more than a factor of 1000 when fluorophores are properly placed near nanoantennas [75–79]. In this technique, in addition to the increase in the absorption cross-section, the radiative decay rate is also increased more

than 10 times. The shortened radiative decay time makes this method more promising because the photon detection rate is ultimately limited to the inverse of the fluorescence lifetime. Further enhancement of photon emission will be possible by much more rapid excitation and radiation cycling. One problem in this method is that the energy transfer rate is not enhanced as much as the radiative decay, which will lower the FRET efficiency [80]. Therefore, it will be more useful for the system with high FRET efficiencies before the enhancement. The control of nano-environment will also be critical for obtaining the same enhancement for every molecule.

There is no photophysics issue in force spectroscopy. Once a molecule is trapped, a long trajectory with a large number of transitions can be recorded without loss of information. However, slow diffusion of beads makes it difficult to further improve the time resolution. Moreover, increasing the viscosity will slow the motions of the beads. In single molecule optical tweezer experiments, it is important to extract the molecular extension from the bead positions that is actually measured. If the bead diffusion is too slow compared to the timescale of the change in molecular extension, the data does not reflect the dynamics of the molecular process. This is problematic for the measurement of transition paths, where the beads should rapidly follow the change of molecular extension, compared to the measurement of rates, where beads can slowly diffuse and catch up to molecular changes during long waiting times in, say, the folded state after a rapid transition. Cassio *et al*. have shown that when the bead diffusion is comparable to the molecular diffusion, the transition path time would be overestimated by ~ 4 fold, while it is possible to obtain an accurate rate coefficient after a linker correction even when the bead diffusion is several orders of magnitude slower than the diffusion of the molecular extension [66]. Currently, the direct measurement of the transition path times is limited to molecules with relatively long transition path times such as DNA hairpins. Further improvement of the time resolution will be possible by using smaller beads, but the force precision will decrease. Similarly, in atomic force microscopy, the ultrashort cantilever with a high time resolution shows moderate force stability [59].

If the improvement of the time resolution leads to the measurement of the distribution of transition path times of more systems, it will be possible to make an interesting comparison. Fig. 2b shows not only the transition path time distributions of different barrier heights but also the distributions for the case that there are intermediate states. Even for apparently two-state systems, it is not unexpected to have some high-energy intermediate states on the barrier. The shape of the distribution depends on the number of intermediate states. If the measurement becomes more accurate, it will be possible to distinguish different cases.

From the three-dimensional structural information obtained during transitions, it will be possible to characterize transition paths in more detail by probing the heterogeneity. Even though a system can be described well by diffusion on a 1D free-energy surface, each transition would look different because of the multi-dimensional nature of the problem. For example, a large modulation of the relative flux in parallel folding pathways has been observed in a combined chemical and mechanical denaturation study of a small protein SH3 domain [81,82]. Cluster analysis of MD trajectories has also shown that some proteins such as ubiquitin follow a quite regular pathway while others fold via diverse routes [18,83,84]. In the folding simulation of villin, a 35-residue protein consists of three α helices, the order of helix formation was found to be very heterogeneous [85,86]. Since the distribution of the order of helix formation also depends on the force field [85], experimental measurement would help to refine the force field. For this purpose, 3-color FRET is a promising tool [87–93]. By measuring the three distances at the same time, it will be possible to determine whether one part of a molecule folds earlier or later than the other part. In single molecule force experiments, stretching more than one direction simultaneously by holding more than two positions of a molecule may provide multi-dimensional information [94,95]. Fluorescence and force methods can also be combined to monitor multiple distances [93,96–105].

Acknowledgements

I thank William Eaton for his guidance in all of the single molecule fluorescence work described in this review and Attila Szabo, Irina Gopich, and Michael Woodside for numerous discussions and many helpful comments on the manuscript. This work was supported by the Intramural Research Program of the National Institute of Diabetes and Digestive and Kidney Diseases, NIH.

References

[1] J.D. Bryngelson, P.G. Wolynes, Intermediates and barrier crossing in a random energy model (with applications to protein folding), J. Phys. Chem. 93 (1989) 6902–6915. doi:10.1021/j100356a007.

[2] N.D. Socci, J.N. Onuchic, P.G. Wolynes, Diffusive dynamics of the reaction coordinate for protein folding funnels, J. Chem. Phys. 104 (1998) 5860–5868. doi:10.1063/1.471317.

[3] D.K. Klimov, D. Thirumalai, Viscosity dependence of the folding rates of proteins, Phys. Rev. Lett. 79 (1997) 317–320. doi:10.1103/PhysRevLett.79.317.

[4] S.S. Plotkin, P.G. Wolynes, Non-Markovian configurational diffusion and reaction coordinates for protein folding, Phys. Rev. Lett. 80 (1998) 5015–5018. doi:10.1103/PhysRevLett.80.5015.

[5] R.B. Best, G. Hummer, Reaction coordinates and rates from transition paths., Proc. Natl. Acad. Sci. U. S. A. 102 (2005) 6732–6737. doi:10.1073/pnas.0408098102.

[6] R.B. Best, G. Hummer, Diffusion models of protein folding, Phys. Chem. Chem. Phys. 13 (2011) 16902–16911. doi:10.1039/c1cp21541h.

[7] W. Zheng, R.B. Best, Reduction of all-atom protein folding dynamics to one-dimensional diffusion, J. Phys. Chem. B. 119 (2015) 15247–15255. doi:10.1021/acs.jpcb.5b09741.

[8] H.S. Chung, S. Piana-Agostinetti, D.E. Shaw, W.A. Eaton, Structural origin of slow diffusion in protein folding, Science. 349 (2015) 1504–1510. doi:10.1126/science.aab1369.

[9] H.S. Chung, W.A. Eaton, Single-molecule fluorescence probes dynamics of barrier crossing., Nature. 502 (2013) 685–8. doi:10.1038/nature12649.

[10] H.A. Kramers, Brownian motion in a field of force and the diffusion model of chemical

reactions, Physica. 7 (1940) 284–304. doi:10.1016/S0031-8914(40)90098-2.

[11] A.R. Fersht, A. Matouschek, L. Serrano, The folding of an enzyme: I. Theory of protein engineering analysis of stability and pathway of protein folding, J. Mol. Biol. 224 (1992) 771–782. doi:10.1016/0022-2836(92)90561-W.

[12] L.S. Itzhaki, D.E. Otzen, A.R. Fersht, The structure of the transition state for folding of chymotrypsin inhibitor 2 analysed by protein engineering methods: Evidence for a nucleation-condensation mechanism for protein folding, J. Mol. Biol. 254 (1995) 260–288. doi:10.1006/jmbi.1995.0616.

[13] A.R. Fersht, Characterizing transition states in protein folding: an essential step in the puzzle, Curr. Opin. Struct. Biol. 5 (1995) 79–84. doi:10.1016/0959-440X(95)80012-P.

[14] S.E. Jackson, How do small single-domain proteins fold?, Fold. Des. 3 (1998) R81–R91. doi:10.1016/S1359-0278(98)00033-9.

[15] B. Schuler, W.A. Eaton, Protein folding studied by single-molecule FRET., Curr. Opin. Struct. Biol. 18 (2008) 16–26. doi:10.1016/j.sbi.2007.12.003.

[16] H.S. Chung, J.M. Louis, W.A. Eaton, Experimental determination of upper bound for transition path times in protein folding from single-molecule photon-by-photon trajectories., Proc. Natl. Acad. Sci. U. S. A. 106 (2009) 11837–11844. doi:10.1073/pnas.0901178106.

[17] D.E. Shaw, P. Maragakis, K. Lindorff-Larsen, S. Piana, R.O. Dror, M.P. Eastwood, J.A. Bank, J.M. Jumper, J.K. Salmon, Y. Shan, W. Wriggers, Atomic-level characterization of the structural dynamics of proteins., Science. 330 (2010) 341–346. doi:10.1126/science.1187409.

[18] K. Lindorff-Larsen, S. Piana, R.O. Dror, D.E. Shaw, How fast-folding proteins fold, Science. 334 (2011) 517–520. doi:10.1126/science.1208351.

[19] G. Hummer, From transition paths to transition states and rate coefficients, J. Chem.

Phys. 120 (2004) 516–523. doi:10.1063/1.1630572.

[20] H.S. Chung, I.V. Gopich, Fast single-molecule FRET spectroscopy: theory and experiment., Phys. Chem. Chem. Phys. 34 (2014) 18644–18657. doi:10.1039/c4cp02489c.

[21] B.W. Zhang, D. Jasnow, D.M. Zuckerman, Transition-event durations in one-dimensional activated processes, J. Chem. Phys. 126 (2007) 74504. doi:10.1063/1.2434966.

[22] H.S. Chung, K. McHale, J.M. Louis, W.A. Eaton, Single-Molecule fluorescence experiments determine protein folding transition path times, Science. 335 (2012) 981–984. doi:10.1126/science.1215768.

[23] I.V. Gopich, A. Szabo, Decoding the pattern of photon colors in single-molecule FRET., J. Phys. Chem. B. 113 (2009) 10965–10973. doi:10.1021/jp903671p.

[24] W.Y. Yang, M. Gruebele, Folding at the speed limit, Nature. 423 (2003) 193–197. doi:10.1038/nature01609.

[25] F. Liu, M. Nakaema, M. Gruebele, The transition state transit time of WW domain folding is controlled by energy landscape roughness, J. Chem. Phys. 131 (2009) 195101. doi:10.1063/1.3262489.

[26] S.J. Hagen, J. Hofrichter, A. Szabo, W.A. Eaton, Diffusion-limited contact formation in unfolded cytochrome c: estimating the maximum rate of protein folding., Proc. Natl. Acad. Sci. U. S. A. 93 (1996) 11615–11617. http://www.ncbi.nlm.nih.gov/pubmed/8876184 (accessed March 19, 2017).

[27] J. Kubelka, J. Hofrichter, W.A. Eaton, The protein folding “speed limit,” Curr. Opin. Struct. Biol. 14 (2004) 76–88. doi:10.1016/j.sbi.2004.01.013.

[28] B. Schuler, E.A. Lipman, W.A. Eaton, Probing the free-energy surface for protein folding with single-molecule fluorescence spectroscopy, Nature. 419 (2002) 743–747.

doi:10.1038/nature01060.

[29] D. Nettels, I. V Gopich, A. Hoffmann, B. Schuler, Ultrafast dynamics of protein collapse from single-molecule photon statistics., Proc. Natl. Acad. Sci. U. S. A. 104 (2007) 2655–60. doi:10.1073/pnas.0611093104.

[30] D. Nettels, A. Hoffmann, B. Schuler, Unfolded protein and peptide dynamics investigated with single-molecule FRET and correlation spectroscopy from picoseconds to seconds., J. Phys. Chem. B. 112 (2008) 6137–46. doi:10.1021/jp076971j.

[31] A. Ansari, C. Jones, E. Henry, J. Hofrichter, W. Eaton, The role of solvent viscosity in the dynamics of protein conformational changes, Science. 256 (1992) 1796–1798. doi:10.1126/science.1615323.

[32] S. J. Hagen, Solvent viscosity and friction in protein folding dynamics, Curr. Protein Pept. Sci. 11 (2010) 385–395. doi:10.2174/138920310791330596.

[33] J.J. Portman, S. Takada, P.G. Wolynes, Microscopic theory of protein folding rates. II. Local reaction coordinates and chain dynamics, J. Chem. Phys. 114 (2001) 5082–5096. doi:10.1063/1.1334663.

[34] D.E. Makarov, Interplay of non-Markov and internal friction effects in the barrier crossing kinetics of biopolymers: Insights from an analytically solvable model, J. Chem. Phys. 138 (2013) 14102. doi:10.1063/1.4773283.

[35] G.S. Jas, W.A. Eaton, J. Hofrichter, Effect of viscosity on the kinetics of α-helix and β-hairpin formation, J. Phys. Chem. B. 105 (2001) 261–272. doi:10.1021/JP0022048.

[36] L. Qiu, S.J. Hagen, A limiting speed for protein folding at low solvent viscosity, J. Am. Chem. Soc. 126 (2004) 3398–3399. doi:10.1021/JA049966R.

[37] T. Cellmer, E.R. Henry, J. Hofrichter, W.A. Eaton, Measuring internal friction of an ultrafast-folding protein., Proc. Natl. Acad. Sci. U. S. A. 105 (2008) 18320–18325.

doi:10.1073/pnas.0806154105.

[38] B.G. Wensley, S. Batey, F.A.C. Bone, Z.M. Chan, N.R. Tumelty, A. Steward, L.G. Kwa, A. Borgia, J. Clarke, Experimental evidence for a frustrated energy landscape in a three-helix-bundle protein family, Nature. 463 (2010) 685–688. doi:10.1038/nature08743.

[39] B.G. Wensley, L.G. Kwa, S.L. Shammas, J.M. Rogers, S. Browning, Z. Yang, J. Clarke, Separating the effects of internal friction and transition state energy to explain the slow, frustrated folding of spectrin domains., Proc. Natl. Acad. Sci. U. S. A. 109 (2012) 17795–17799. doi:10.1073/pnas.1201793109.

[40] A. Borgia, B.G. Wensley, A. Soranno, D. Nettels, M.B. Borgia, A. Hoffmann, S.H. Pfeil, E.A. Lipman, J. Clarke, B. Schuler, Localizing internal friction along the reaction coordinate of protein folding by combining ensemble and single-molecule fluorescence spectroscopy, Nat. Commun. 3 (2012) 1195. doi:10.1038/ncomms2204.

[41] J.D. Bryngelson, J.N. Onuchic, N.D. Socci, P.G. Wolynes, Funnels, pathways, and the energy landscape of protein folding: A synthesis, Proteins Struct. Funct. Genet. 21 (1995) 167–195. doi:10.1002/prot.340210302.

[42] R.B. Best, G. Hummer, W.A. Eaton, Native contacts determine protein folding mechanisms in atomistic simulations., Proc. Natl. Acad. Sci. U. S. A. 110 (2013) 17874–17879. doi:10.1073/pnas.1311599110.

[43] D. de Sancho, A. Sirur, R.B. Best, Molecular origins of internal friction effects on protein-folding rates, Nat. Commun. 5 (2014) 174105. doi:10.1038/ncomms5307.

[44] R.F. Grote, J.T. Hynes, The stable states picture of chemical reactions. II. Rate constants for condensed and gas phase reaction models, J. Chem. Phys. 73 (1980) 2715–2732. doi:10.1063/1.440485.

[45] S.P. Velsko, D.H. Waldeck, G.R. Fleming, Breakdown of Kramers theory description of

photochemical isomerization and the possible involvement of frequency dependent friction, J. Chem. Phys. 78 (1983) 249–258. doi:10.1063/1.444549.

[46] W. Zheng, D. de Sancho, R.B. Best, Modulation of folding internal friction by local and global barrier heights, J. Phys. Chem. Lett. 7 (2016) 1028–1034. doi:10.1021/acs.jpclett.6b00329.

[47] W. Zheng, D. De Sancho, T. Hoppe, R.B. Best, Dependence of internal friction on folding mechanism, J. Am. Chem. Soc. 137 (2015) 3283–3290. doi:10.1021/ja511609u.

[48] G. Hummer, A. Szabo, Free energy reconstruction from nonequilibrium single-molecule pulling experiments., Proc. Natl. Acad. Sci. U. S. A. 98 (2001) 3658–3661. doi:10.1073/pnas.071034098.

[49] M.T. Woodside, P.C. Anthony, W.M. Behnke-Parks, K. Larizadeh, D. Herschlag, S.M. Block, Direct measurement of the full, sequence-dependent folding landscape of a nucleic acid, Science. 314 (2006) 1001–1004. doi:10.1126/science.1133601.

[50] G. Hummer, A. Szabo, Free energy profiles from single-molecule pulling experiments., Proc. Natl. Acad. Sci. U. S. A. 107 (2010) 21441–21446. doi:10.1073/pnas.1015661107.

[51] M.C. Engel, D.B. Ritchie, D.A.N. Foster, K.S.D. Beach, M.T. Woodside, Reconstructing folding energy landscape profiles from nonequilibrium pulling curves with an inverse Weierstrass integral transform, Phys. Rev. Lett. 113 (2014) 238104. doi:10.1103/PhysRevLett.113.238104.

[52] M.T. Woodside, S.M. Block, Reconstructing folding energy landscapes by single-molecule force spectroscopy, Annu. Rev. Biophys. 43 (2014) 19–39. doi:10.1146/annurev-biophys-051013-022754.

[53] A.N. Gupta, A. Vincent, K. Neupane, H. Yu, F. Wang, M.T. Woodside, Experimental validation of free-energy-landscape reconstruction from non-equilibrium single-molecule

force spectroscopy measurements, Nat. Phys. 7 (2011) 631–634. doi:10.1038/nphys2022.

[54] K. Neupane, D.B. Ritchie, H. Yu, D.A.N. Foster, F. Wang, M.T. Woodside, Transition path times for nucleic acid folding determined from energy-landscape analysis of single-molecule trajectories, Phys. Rev. Lett. 109 (2012) 68102. doi:10.1103/PhysRevLett.109.068102.

[55] H. Yu, A.N. Gupta, X. Liu, K. Neupane, A.M. Brigley, I. Sosova, M.T. Woodside, Energy landscape analysis of native folding of the prion protein yields the diffusion constant, transition path time, and rates., Proc. Natl. Acad. Sci. U. S. A. 109 (2012) 14452–14457. doi:10.1073/pnas.1206190109.

[56] K. Truex, H.S. Chung, J.M. Louis, W.A. Eaton, Testing landscape theory for biomolecular processes with single molecule fluorescence spectroscopy, Phys. Rev. Lett. 115 (2015) 18101. doi:10.1103/PhysRevLett.115.018101.

[57] Y.M. Rhee, V.S. Pande, One-dimensional reaction coordinate and the corresponding potential of mean force from commitment probability distribution, J. Phys. Chem. B. 109 (2005) 6780–6786. doi:10.1021/JP045544S.

[58] A.P. Manuel, J. Lambert, M.T. Woodside, Reconstructing folding energy landscapes from splitting probability analysis of single-molecule trajectories., Proc. Natl. Acad. Sci. U. S. A. 112 (2015) 7183–7188. doi:10.1073/pnas.1419490112.

[59] D.T. Edwards, T.T. Perkins, Optimizing force spectroscopy by modifying commercial cantilevers: Improved stability, precision, and temporal resolution, J. Struct. Biol. 197 (2017) 13–25. doi:10.1016/j.jsb.2016.01.009.

[60] H. Yu, M.G.W. Siewny, D.T. Edwards, A.W. Sanders, T.T. Perkins, Hidden dynamics in the unfolding of individual bacteriorhodopsin proteins, Science. 355 (2017) 945–950. http://science.sciencemag.org/content/355/6328/945.long (accessed March 28, 2017).

[61] K. Neupane, D.A.N. Foster, D.R. Dee, H. Yu, F. Wang, M.T. Woodside, Direct observation of transition paths during the folding of proteins and nucleic acids, Science. 352 (2016) 239–242. doi:10.1126/science.aad0637.

[62] H. Yu, D.R. Dee, X. Liu, A.M. Brigley, I. Sosova, M.T. Woodside, Protein misfolding occurs by slow diffusion across multiple barriers in a rough energy landscape., Proc. Natl. Acad. Sci. U. S. A. 112 (2015) 8308–8313. doi:10.1073/pnas.1419197112.

[63] K. Neupane, F. Wang, M.T. Woodside, Direct measurement of sequence-dependent transition path times and conformational diffusion in DNA duplex formation., Proc. Natl. Acad. Sci. U. S. A. 114 (2017) 1329–1334. doi:10.1073/pnas.1611602114.

[64] M. Hinczewski, Y. von Hansen, R.R. Netz, Deconvolution of dynamic mechanical networks., Proc. Natl. Acad. Sci. U. S. A. 107 (2010) 21493–21498. doi:10.1073/pnas.1010476107.

[65] G.-M. Nam, D.E. Makarov, Extracting intrinsic dynamic parameters of biomolecular folding from single-molecule force spectroscopy experiments, Protein Sci. 25 (2016) 123–134. doi:10.1002/pro.2727.

[66] P. Cossio, G. Hummer, A. Szabo, On artifacts in single-molecule force spectroscopy., Proc. Natl. Acad. Sci. U. S. A. 112 (2015) 14248–14253. doi:10.1073/pnas.1519633112.

[67] K. Neupane, M.T. Woodside, Quantifying instrumental artifacts in folding kinetics measured by single-molecule force spectroscopy, Biophys. J. 111 (2016) 283–286. doi:10.1016/j.bpj.2016.06.011.

[68] E. Pollak, Transition path time distribution and the transition path free energy barrier, Phys. Chem. Chem. Phys. 18 (2016) 28872–28882. doi:10.1039/C6CP05052B.

[69] D.E. Makarov, Reconciling transition path time and rate measurements in reactions with large entropic barriers, J. Chem. Phys. 146 (2017) 71101. doi:10.1063/1.4977177.

[70] H.S. Chung, T. Cellmer, J.M. Louis, W.A. Eaton, Measuring ultrafast protein folding rates from photon-by-photon analysis of single molecule fluorescence trajectories, Chem. Phys. 422 (2013) 229–237. doi:10.1016/j.chemphys.2012.08.005.

[71] H.S. Chung, J.M. Louis, I.V. Gopich, Analysis of fluorescence lifetime and energy transfer efficiency in single-molecule photon trajectories of fast-folding proteins, J. Phys. Chem. B. 120 (2016) 680–699. doi:10.1021/acs.jpcb.5b11351.

[72] M.F. Juette, D.S. Terry, M.R. Wasserman, Z. Zhou, R.B. Altman, Q. Zheng, S.C. Blanchard, The bright future of single-molecule fluorescence imaging, Curr. Opin. Chem. Biol. 20 (2014) 103–111. doi:10.1016/j.cbpa.2014.05.010.

[73] Q. Zheng, M.F. Juette, S. Jockusch, M.R. Wasserman, Z. Zhou, R.B. Altman, S.C. Blanchard, Ultra-stable organic fluorophores for single-molecule research, Chem. Soc. Rev. 43 (2014) 1044–1056. doi:10.1039/C3CS60237K.

[74] J.H.M. van der Velde, J. Oelerich, J. Huang, J.H. Smit, M. Hiermaier, E. Ploetz, A. Herrmann, G. Roelfes, T. Cordes, The power of two: Covalent coupling of photostabilizers for fluorescence applications, J. Phys. Chem. Lett. 5 (2014) 3792–3798. doi:10.1021/jz501874f.

[75] A. Kinkhabwala, Z. Yu, S. Fan, Y. Avlasevich, K. Müllen, W.E. Moerner, Large single-molecule fluorescence enhancements produced by a bowtie nanoantenna, Nat. Photonics. 3 (2009) 654–657. doi:10.1038/nphoton.2009.187.

[76] G.P. Acuna, F.M. Möller, P. Holzmeister, S. Beater, B. Lalkens, P. Tinnefeld, Fluorescence enhancement at docking sites of DNA-directed self-assembled nanoantennas, Science. 338 (2012) 506–510. http://science.sciencemag.org/content/338/6106/506 (accessed April 7, 2017).

[77] H. Yuan, S. Khatua, P. Zijlstra, M. Yorulmaz, M. Orrit, Thousand-fold enhancement of

single-molecule fluorescence near a single gold nanorod, Angew. Chemie Int. Ed. 52 (2013) 1217–1221. doi:10.1002/anie.201208125.

[78] D. Punj, M. Mivelle, S.B. Moparthi, T.S. van Zanten, H. Rigneault, N.F. van Hulst, M.F. García-Parajó, J. Wenger, A plasmonic “antenna-in-box” platform for enhanced single-molecule analysis at micromolar concentrations, Nat. Nanotechnol. 8 (2013) 512–516. doi:10.1038/nnano.2013.98.

[79] E. Wientjes, J. Renger, A.G. Curto, R. Cogdell, N.F. van Hulst, Strong antenna-enhanced fluorescence of a single light-harvesting complex shows photon antibunching, Nat. Commun. 5 (2014) 1516–1519. doi:10.1038/ncomms5236.

[80] S. Bidault, A. Devilez, P. Ghenuche, B. Stout, N. Bonod, J. Wenger, Competition between Förster Resonance Energy Transfer and Donor Photodynamics in Plasmonic Dimer Nanoantennas, ACS Photonics. 3 (2016) 895–903. doi:10.1021/acsphotonics.6b00148.

[81] E.J. Guinn, B. Jagannathan, S. Marqusee, S. Marqusee, C. Bustamante, Single-molecule chemo-mechanical unfolding reveals multiple transition state barriers in a small single-domain protein, Nat. Commun. 6 (2015) 6861. doi:10.1038/ncomms7861.

[82] P.I. Zhuravlev, M. Hinczewski, S. Chakrabarti, S. Marqusee, D. Thirumalai, Force-dependent switch in protein unfolding pathways and transition-state movements., Proc. Natl. Acad. Sci. U. S. A. 113 (2016) E715-724. doi:10.1073/pnas.1515730113.

[83] S. Piana, K. Lindorff-Larsen, D.E. Shaw, Atomic-level description of ubiquitin folding., Proc. Natl. Acad. Sci. U. S. A. 110 (2013) 5915–5920. doi:10.1073/pnas.1218321110.

[84] R.B. Best, G. Hummer, Microscopic interpretation of folding ϕ-values using the transition path ensemble., Proc. Natl. Acad. Sci. U. S. A. 113 (2016) 3263–3268. doi:10.1073/pnas.1520864113.

[85] S. Piana, K. Lindorff-Larsen, D.E. Shaw, E. Al., How robust are protein folding

simulations with respect to force field parameterization?, Biophys. J. 100 (2011) L47–L49. doi:10.1016/j.bpj.2011.03.051.

[86] E.R. Henry, R.B. Best, W.A. Eaton, Comparing a simple theoretical model for protein folding with all-atom molecular dynamics simulations., Proc. Natl. Acad. Sci. U. S. A. 110 (2013) 17880–17885. doi:10.1073/pnas.1317105110.

[87] S. Hohng, C. Joo, T. Ha, Single-molecule three-color FRET, Biophys. J. 87 (2004) 1328–1337. doi:10.1529/biophysj.104.043935.

[88] N.K. Lee, A.N. Kapanidis, H.R. Koh, Y. Korlann, S.O. Ho, Y. Kim, N. Gassman, S.K. Kim, S. Weiss, Three-color alternating-laser excitation of single molecules: monitoring multiple interactions and distances., Biophys. J. 92 (2007) 303–312. doi:10.1529/biophysj.106.093211.

[89] Y. Gambin, A.A. Deniz, Multicolor single-molecule FRET to explore protein folding and binding., Mol. Biosyst. 6 (2010) 1540–7. doi:10.1039/c003024d.

[90] J. Ross, P. Buschkamp, D. Fetting, A. Donnermeyer, C.M. Roth, P. Tinnefeld, Multicolor single-molecule spectroscopy with alternating laser excitation for the investigation of interactions and dynamics., J. Phys. Chem. B. 111 (2007) 321–326. doi:10.1021/jp066082g.

[91] J. Lee, S. Lee, K. Ragunathan, C. Joo, T. Ha, S. Hohng, Single-molecule four-color FRET, Angew. Chemie Int. Ed. 49 (2010) 9922–9925. doi:10.1002/anie.201005402.

[92] C. Ratzke, B. Hellenkamp, T. Hugel, Four-colour FRET reveals directionality in the Hsp90 multicomponent machinery, Nat. Commun. 5 (2014) 309–321. doi:10.1038/ncomms5192.

[93] S. Hohng, S. Lee, J. Lee, M.H. Jo, Maximizing information content of single-molecule FRET experiments: multi-color FRET and FRET combined with force or torque, Chem. Soc. Rev. 43 (2014) 1007–1013. doi:10.1039/C3CS60184F.

[94] R.T. Dame, M.C. Noom, G.J.L. Wuite, Bacterial chromatin organization by H-NS protein unravelled using dual DNA manipulation, Nature. 444 (2006) 387–390. doi:10.1038/nature05283.

[95] J.T. Inman, B.Y. Smith, M.A. Hall, R.A. Forties, J. Jin, J.P. Sethna, M.D. Wang, DNA Y structure: A versatile, multidimensional single molecule assay, Nano Lett. 14 (2014) 6475–6480. doi:10.1021/nl503009d.

[96] S. Hohng, R. Zhou, M.K. Nahas, J. Yu, K. Schulten, D.M.J. Lilley, T. Ha, Fluorescence-force spectroscopy maps two-dimensional reaction landscape of the Holliday junction, Science. 318 (2007) 279–283. http://science.sciencemag.org/content/318/5848/279 (accessed April 6, 2017).

[97] G. Sirinakis, Y. Ren, Y. Gao, Z. Xi, Y. Zhang, Combined versatile high-resolution optical tweezers and single-molecule fluorescence microscopy, Rev. Sci. Instrum. 83 (2012) 93708. doi:10.1063/1.4752190.

[98] S. Lee, S. Hohng, An optical trap combined with three-color FRET, J. Am. Chem. Soc. 135 (2013) 18260–18263. doi:10.1021/ja408767p.

[99] X. Long, J.W. Parks, C.R. Bagshaw, M.D. Stone, Mechanical unfolding of human telomere G-quadruplex DNA probed by integrated fluorescence and magnetic tweezers spectroscopy, Nucleic Acids Res. 41 (2013) 2746–2755. doi:10.1093/nar/gks1341.

[100] M. Lee, S.H. Kim, S.-C. Hong, Minute negative superhelicity is sufficient to induce the B-Z transition in the presence of low tension., Proc. Natl. Acad. Sci. U. S. A. 107 (2010) 4985–4990. doi:10.1073/pnas.0911528107.

[101] F.E. Kemmerich, M. Swoboda, D.J. Kauert, M.S. Grieb, S. Hahn, F.W. Schwarz, R. Seidel, M. Schlierf, Simultaneous single-molecule force and fluorescence sampling of DNA nanostructure conformations using magnetic tweezers, Nano Lett. 16 (2016) 381–

386. doi:10.1021/acs.nanolett.5b03956.

[102] Y. He, M. Lu, J. Cao, H.P. Lu, Manipulating protein conformations by single-molecule AFM-FRET nanoscopy, ACS Nano. 6 (2012) 1221–1229. doi:10.1021/nn2038669.

[103] J.C. Cordova, D.K. Das, H.W. Manning, M.J. Lang, Combining single-molecule manipulation and single-molecule detection, Curr. Opin. Struct. Biol. 28 (2014) 142–148. doi:10.1016/j.sbi.2014.08.010.

[104] M.J. Comstock, K.D. Whitley, H. Jia, J. Sokoloski, T.M. Lohman, T. Ha, Y.R. Chemla, Direct observation of structure-function relationship in a nucleic acid–processing enzyme, Science. 348 (2015) 352–354. http://science.sciencemag.org/content/348/6232/352/tab-pdf (accessed April 7, 2017).

[105] Y.R. Chemla, High-resolution, hybrid optical trapping methods, and their application to nucleic acid processing proteins, Biopolymers. 105 (2016) 704–714. doi:10.1002/bip.22880.

Figure Legends

Fig. 1. Free energy surface of protein folding. (a) Protein folding is well described by diffusion on a one-dimensional (1D) free energy surface on which a multi-dimensional (drawn in two-dimension) free energy landscape is projected. Figure is adapted from Ref. [8]. (b) Details of 1D free energy surface. The folded and unfolded states are separated by a free energy barrier with the height of ΔG_f^*. $(\omega_u)^2$, $(\omega_f)^2$, and $(\omega^*)^2$, are curvatures at the bottom of the unfolded and folded state wells and at the top of the barrier, respectively. An unfolded molecule fluctuates in the unfolded well for a relatively long time before making a very rapid folding transition over the barrier. The transition path is the molecular trajectory of barrier crossing between q_u and q_f in the folding reaction coordinate (brown portion of the trajectory). In single molecule fluorescence experiments, the transition path appears as an instantaneous jump between the two states in an idealized FRET efficiency trajectory (FRET efficiencies are 0 and 1 for the unfolded and folded states). If the transition path time is longer than the average photon interval, it is possible to detect the transition path by analyzing individual donor (green) and acceptor (red) photons. Figure is adapted from Ref. [9]. (c) A protein molecule (α_3D) labeled with a donor (Alexa 488) and an acceptor (Alexa 594) dyes. Single molecule fluorescence trajectories are collected from molecules immobilized on a glass surface. Fluorophores are attached so that the inter-dye distance is short when the protein is folded (high FRET efficiency) and long when the protein is unfolded (low FRET efficiency). Figure is taken from Ref. [9].

Fig. 2. Calculation of transition path times for a parabolic barrier. (a) Parabolic barrier with a barrier height of ΔG^*. (b) Comparison of the transition path time distribution at different barrier heights. The solid lines are the distributions calculated using Eq. (4). The dashed lines are the distributions for the cases that there are 1 to 3 intermediate states (S) with an equal lifetime

between the folded and unfolded states. In these cases, the distributions of the apparent transition path time $P(t)$ are: $t_{TP}^{-1}\exp(-t/t_{TP})$ (1S), $4t_{TP}^{-1}\exp[-(8/3)t/t_{TP}]\sinh[(4/3)t/t_{TP}]$ (2S), and $10t_{TP}^{-1}\exp(-5t/t_{TP})\sinh^2[(5/2\sqrt{2})t/t_{TP}]$ (3S) (see Ref. [22]). The distributions are scaled so that their average transition path times are 1 (red vertical dashed line). (c) The barrier height dependence of the average transition path times from Eq. (3) (blue) and the mean value numerically calculated using the probability density function in Eq. (4) (red). The exact values t_{TP} (exact) were calculated using Eq. (2).

Fig. 3. Determination of transition path times of two-state proteins. (a) Donor (green) and acceptor (red) trajectories (50 μs bin time) and photon trajectories near the folding transition of the FBP28 WW domain. (b) In order to determine the transition path time, a virtual intermediate state S was inserted between the folded (F) and unfolded (U) states, and photon trajectories near transitions were analyzed using the maximum likelihood method with the three-state model. The average transition path time is equal to the lifetime of S in this model ($t_{TP} = (2k_S)^{-1}$). (c) The difference of the log likelihood, $\Delta\ln L = \ln L(\tau_S) - \ln L(0)$. $L(0)$ is the likelihood for the two-state model, in which transitions are instantaneous. The transition path time of the WW domain is determined to be 16 μs (at the viscosity of 10 cP), which is the time at the maximum of $\Delta\ln L$. (d) Since no peak is observed in the likelihood plot, only the upper bound of the transition path time of 10 μs is determined for protein G B1 domain. Figures are adapted from Ref. [22].

Fig. 4. Characterization of slow diffusion of α_3D folding by measurement of transition path times using single molecule FRET and all-atom MD simulations. (a) Viscosity- and temperature-dependence of the transition path time at neutral pH. (Left) The orange curve is a fit to the power-law function $A(\eta/\eta_0)^{\alpha}$, with α = 0.30 ± 0.03. The blue line is the viscosity dependence

expected when the transition path time is linearly proportional to the viscosity. (Right) The orange curve is a fit to the super Arrhenius dependence of the diffusion coefficient at the barrier top, $D^* \propto \exp[-(\Delta E/k_BT)^2]$, with $\Delta E = 2.3 \pm 0.4\ k_BT$. The blue curve shows the dependence expected when D^* is linearly proportional to the inverse of the viscosity of the solution. Figures are adapted from Ref. [9]. (b) pH dependence of the relaxation rate ($k = k_f + k_u$) near the mid-point of urea denaturation. (c) The viscosity dependence of the relaxation time ($1/k$) near the mid-point of denaturation at neutral (left) and low (right) pH. The dependences were fitted to either the power-low (orange curves) or a linear equation (green), $A(\sigma + \eta/\eta_0)$, where σ is the internal viscosity. (d) (Top) Snapshots of α_3D conformations in the unfolded state (left), transition path (middle three), and folded state (right). Side chains that are involved in non-native and native salt-bridge formation are indicated in red and blue, respectively. (Bottom) 1D free energy surface (black) and average number of non-native (red) and native (blue) salt bridges along the reaction coordinate r. (e) The average number and persistence times of non-native salt bridges formed between negatively charged residues and either arginine or lysine residues found on the transition paths at pH 7 and 2. (b – e) Figures are adapted from Ref. [8].

Fig. 5. Measurement of transition path times using single molecule force experiments. (a) A DNA hairpin attached by DNA linkers to two beads is stretched by optical tweezers. (b) Reversible folding and unfolding transitions are observed in a trajectory of the total extension (molecule + linker). The time resolution is sufficiently high that the transition paths (red, right) of individual transitions can be measured. (c) The distribution of the transition path times. The distribution is same for the folding (green bars) and unfolding (black bars) transitions as expected from microscopic reversibility. The fits of the whole distribution to Eq. (4) and the tail part to an exponential function (inset) result in the same landscape parameters. Figures are adapted from Ref. [61].

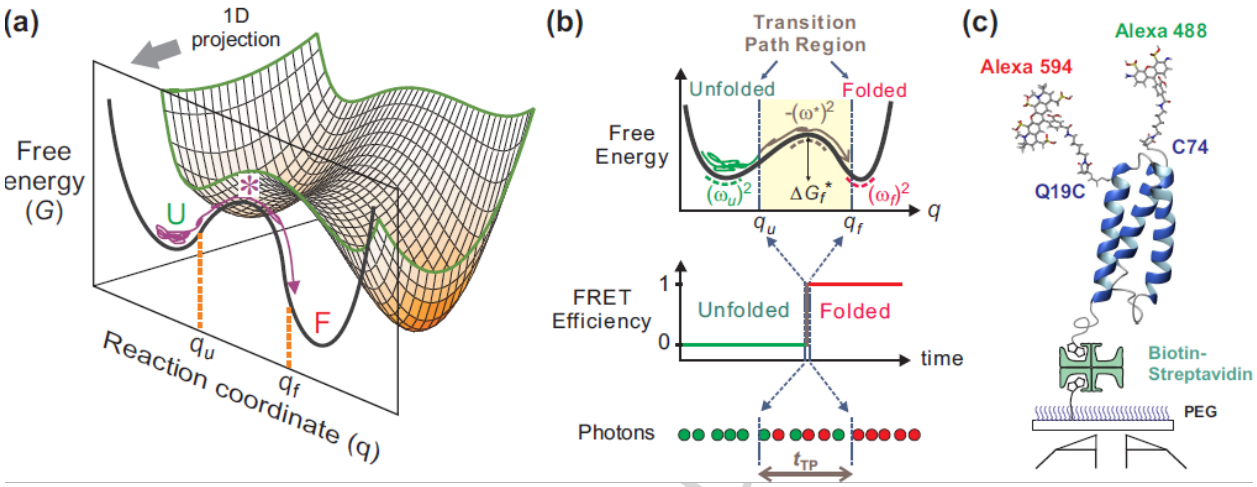

Fig. 1

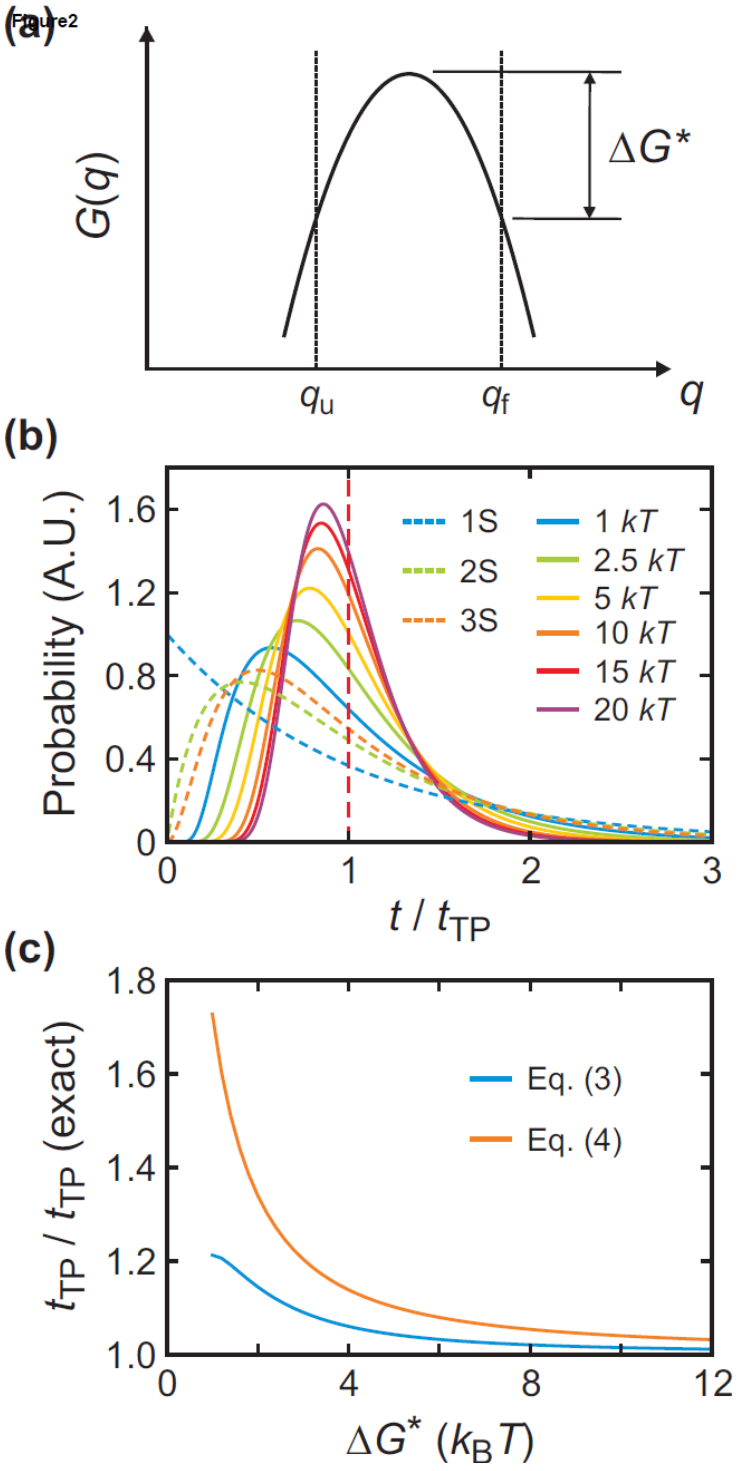

Fig. 2

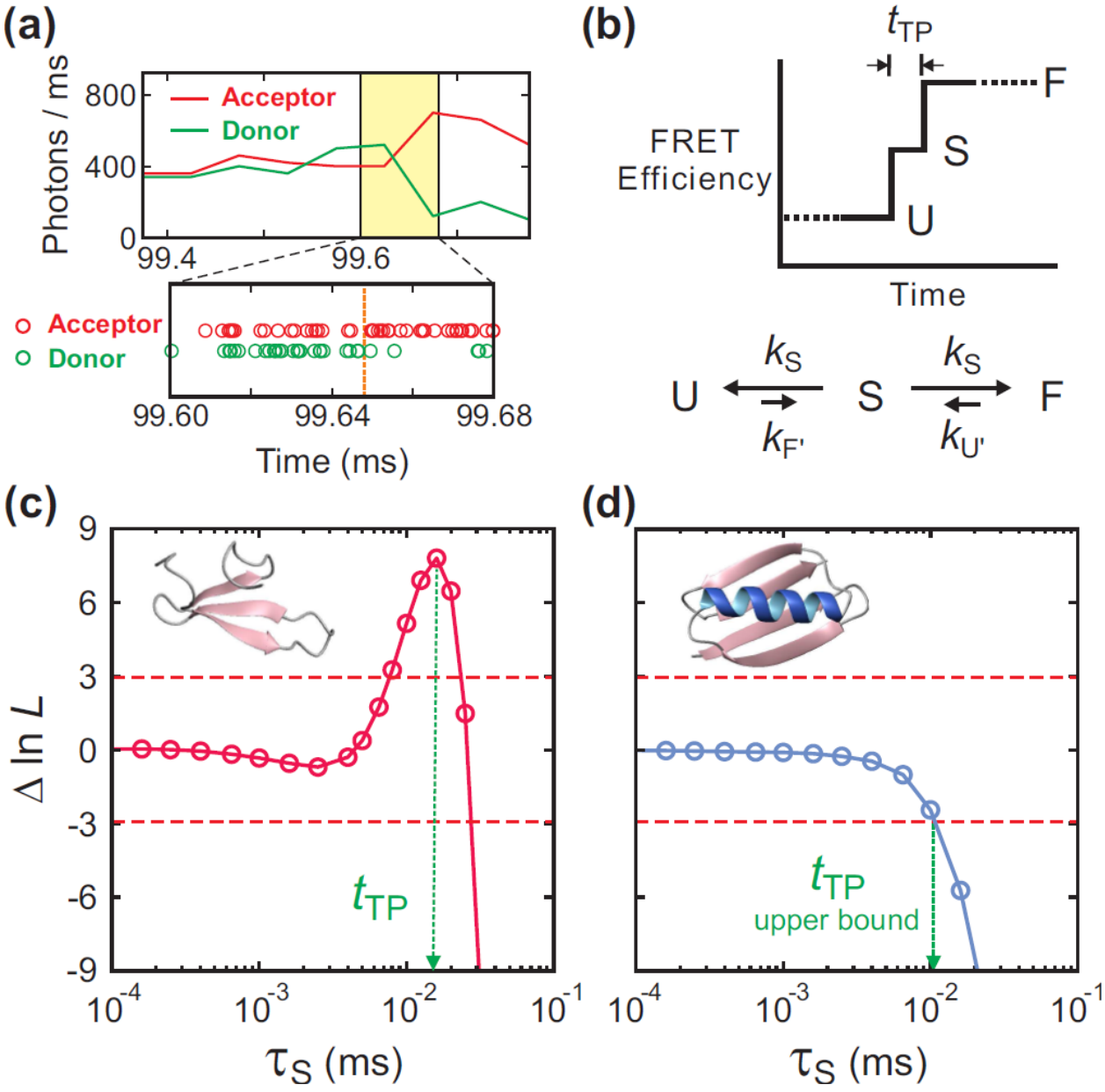

Fig. 3

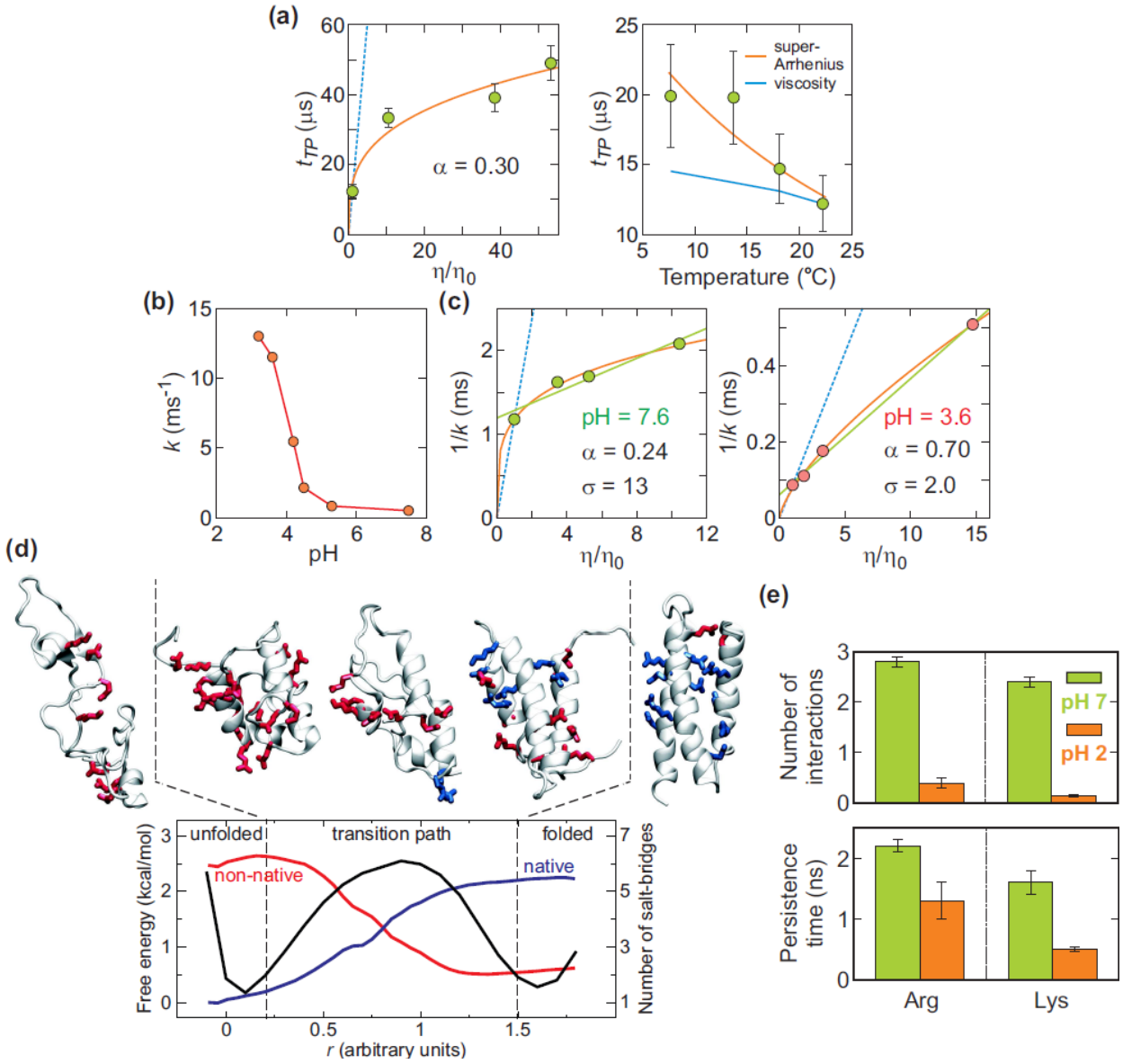

Fig. 4

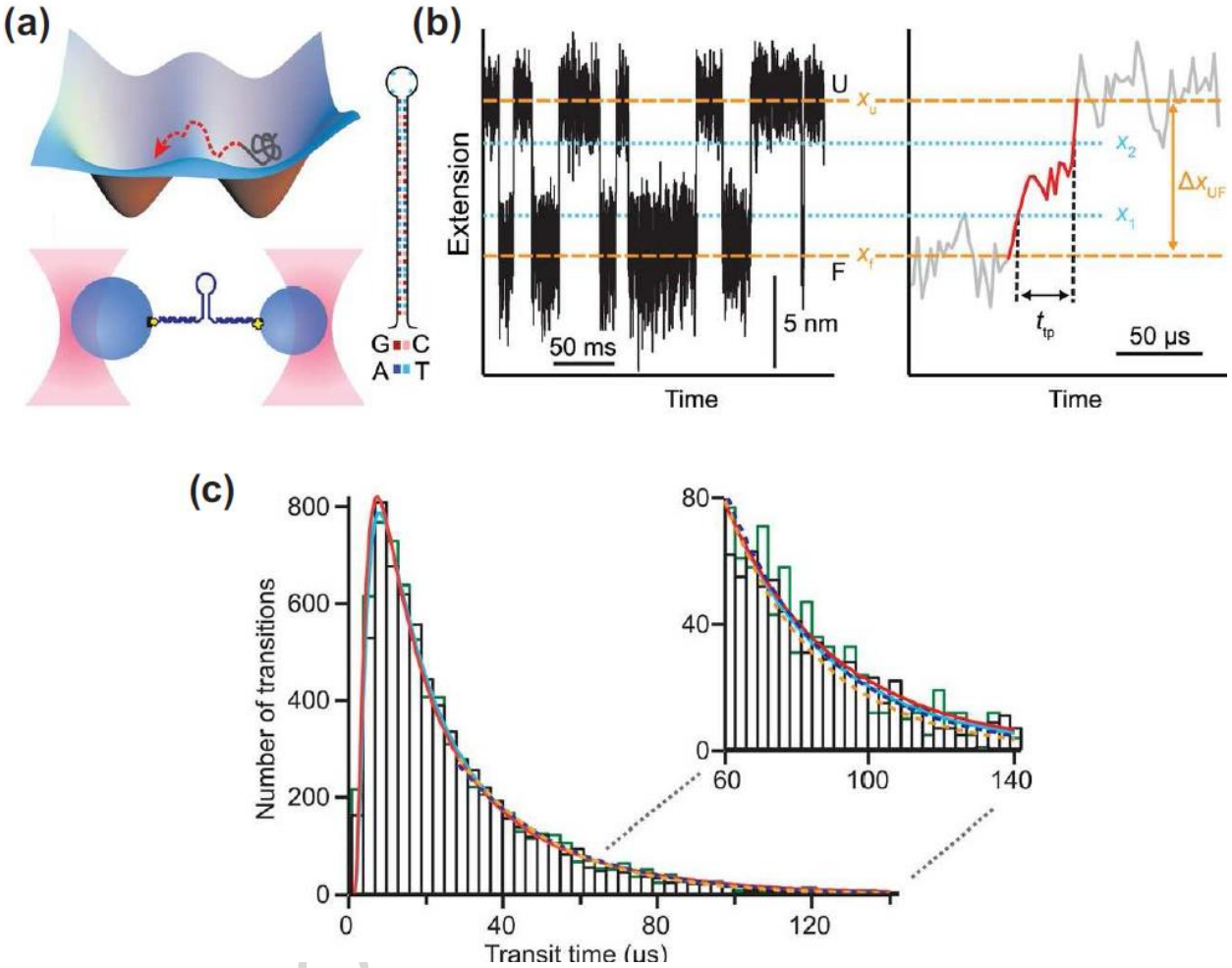

Fig. 5

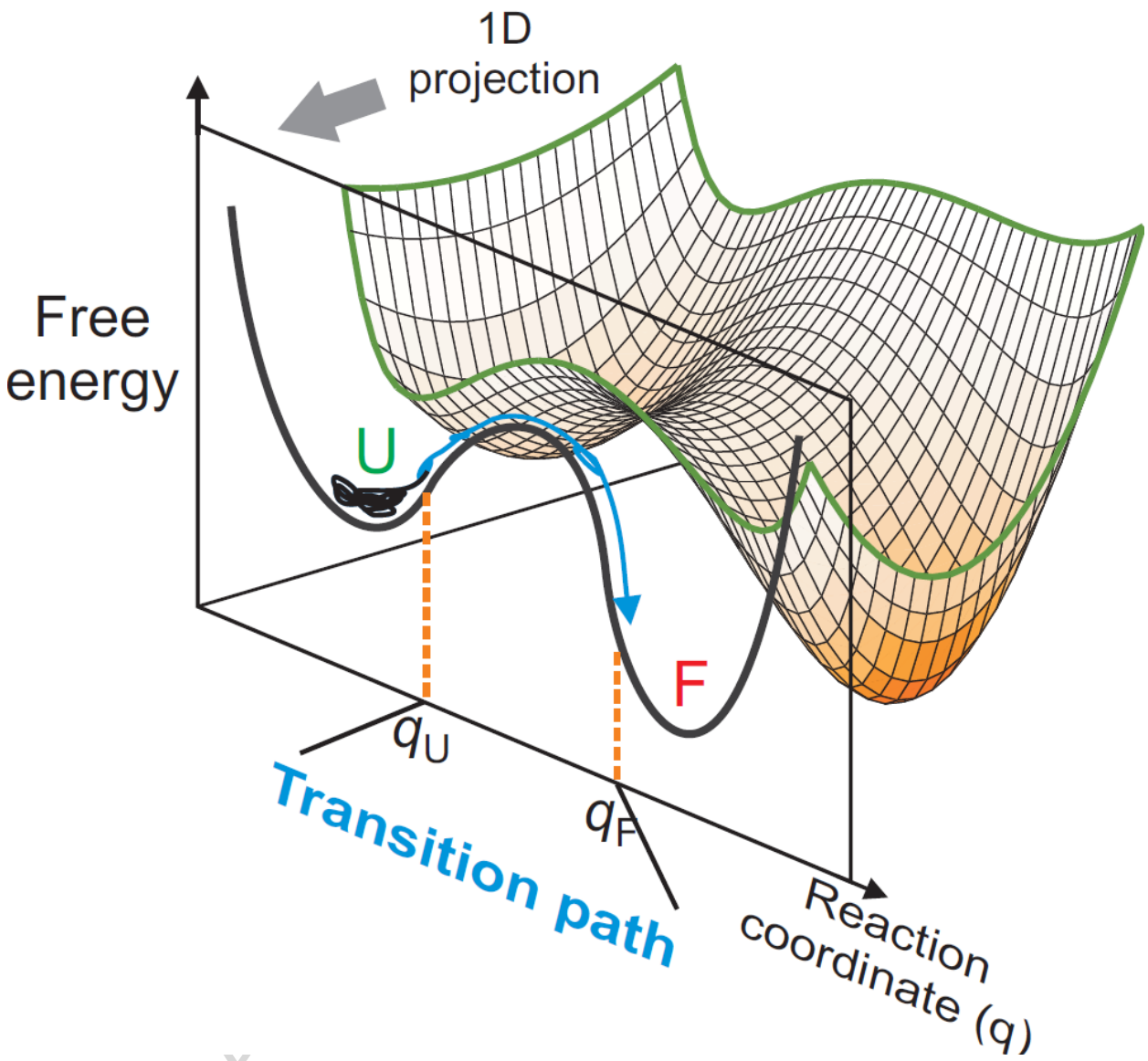

Graphical abstract

Highlights

- Fluorescence experiment determined average transition path times of protein folding
- Transition path time is insensitive to the free energy barrier height
- Transition path time measurement characterized diffusive barrier crossing dynamics
- Transition path analysis validated 1D description of folding of biomolecules
- Single-molecule force spectroscopy measured distributions of transition path times